2022 IEEE/RSJ International Conference on Intelligent Robots and Systems (IROS)
October 23-27, 2022, Kyoto, Japan

The Relationship Between Incremental Changes in Orientation and Slip Speed Estimation Using the Fingerprint Effect*

Robert Kovenburg, *Member, IEEE*, Andrew Slezak, Chase George, Richard Gale, *Senior Member, IEEE,* and Burak Aksak*, Member, IEEE*

Abstract— **The fingerprint effect, wherein vibrations are produced with frequencies related to the speed of a surface sliding across fingerprint ridges and the period of those ridges, has been studied for use in both slip detection and texture recognition. Here, we use a simple bioinspired sensor with parallel, straight, fingerprint-like ridges and a single ferroelectric ceramic transducer to show that the fingerprint effect is orientation dependent and that, if the orientation is known, it can be used to estimate slip speed. Our results, obtained at sliding speeds of 15 mm/s, 20 mm/s, and 25 mm/s and orientations from 0º - 90º, clearly demonstrate this dependence. Additionally, we use our results to run a simulation, using MATLAB software, of real-time slip speed estimation. The simulation shows that the fingerprint effect can be used for real-time slip-speed estimation.**

I. Introduction

It has been shown that the human fingerprint can, when sliding across a surface, convert spatial frequencies to temporal frequencies (vibrations). In this conversion process, fingerprints have a filtering effect whereby they amplify spatial frequencies in a band centered on the fundamental frequency of the prints themselves [1]. That is to say that the frequency of the highest magnitude vibrations produced by the movement of fingerprints across a surface are indirectly related to the spacing of the fingerprint ridges and directly related to the relative (scanning or slip) speed between the prints and the surface they are in contact with. The ability of fingerprints and fingerprint-like structures to amplify vibrations has used to both detect slip and identify textures [2][3][4][5].

Given the relationship between slip speed and the center frequency of the filter created by fingerprint-like structures, one use of the fingerprint effect can be to calculate the slip speed of a surface in contact with said structures. This could be applied to robotics in, for example, active touch for texture identification or controlled slip. A study by Massalim *et al.* used deep learning to detect slip, slip speed, and texture from vibrations [6]. However, fingerprint-like structures, and thus the fingerprint effect, do not appear to have been present in that study. We will show that, when fingerprint-like structures are present, the fingerprint effect can be used to find a good estimate of slip speed.

Additionally, as we will show, structure spacing is orientation dependent in most fingerprint-like structures that are commonly used in tactile sensing applications. There is, in fact, only one structure pattern that, at one contact angle, maintains a constant structure spacing in all directions (evenly spaced concentric circular ridges). As such, it is important to understand how the direction of slip effects the frequencies of the vibrations produced. Several previous studies have examined the frictional relationship between a fingertip and a slipping surface in both the proximal-distal and radial-ulnar directions [7][8]. Oddo *et al.* used a biomimetic sensor to study incremental rotation between 0º and 90º in [9]. To do this, they used a periodic grating as a test surface. The result reflects the frequency of the grating and not the fingerprint-like structures. To the best of our knowledge, the relationship between the fingerprint effect and orientations between 0º and 90º has not been studied, yet.

This paper will show both that the center frequency of the fingerprint effect is orientation dependent, and that, if the orientation is known, it can be used to estimate slip speed in real-time.

II. Theory

A. Effect of Orientation on the Fingerprint Ridge Spacing

The fingerprint effect, as described by Scheibert *et al.* in [1] refers to the way in which surface features interact with the ridges of a sliding fingerprint to elicit vibrations that are sensed by mechanoreceptors in the skin beneath the ridges. The frequencies of vibrations created by this process are at a maximum at a center frequency f_c defined by

$$f_c = v/\lambda, \tag{1}$$

where v is the slip speed of the fingerprint across the surface and λ is the center-to-center spacing of the fingerprint ridges. These vibrations are the result of frictional forces between the surface and the fingerprint [10]. While many factors contribute to these frictional forces, in general, friction increases with increased contact area, which is maximized when the spatial frequency of surface features

*Research supported in part by the National Science Foundation under Grant # 1810402. .

R. Kovenburg is with the Electrical and Computer Engineering Department, Texas Tech University, Lubbock, TX 79409 USA (robert.koven@ttu.edu).

A. Slezak is with the Mechanical Engineering Department, Texas Tech University, Lubbock, TX 79409 USA (aslezak@ttu.edu)

C. George is with the Mechanical Engineering Department, Texas Tech University, Lubbock, TX 79409 USA (chase.r.george@ttu.edu)

R. Gale is with the Electrical & Computer Engineering Department, Texas Tech University, Lubbock TX, 79409 USA (Richard.gale@ttu.edu)

B. Aksak is with the Mechanical Engineering Department, Texas Tech University, Lubbock, TX 79409 USA (burak.aksak@ttu.edu)

matches the spatial frequency of the fingerprint-like ridges. Scheibert *et al.* showed this effect using a sensor with straight, parallel ridges. While the general principal holds for curved fingerprint-like ridges and other fingerprint-like structures, this paper will only address straight, parallel ridges. We chose this ridge configuration because it is commonly used by other researchers, it only requires straightforward analysis, and because curved, evenly spaced ridges with large enough radii of curvature can be approximated as straight, parallel lines.

Given the relationship between fingerprint ridge spacing and vibration frequency, and its reliance on matching the spatial frequencies of surface features, we can picture what happens when we change the orientation of the ridges by rotating them with respect to the direction of movement. As Fig. 1 demonstrates, the spatial period λ of ridges with respect to the direction of movement changes from λ_1 to λ_2 as the orientation of the ridge pattern changes.

To see how the spacing between straight, evenly spaced, parallel lines changes given a rotation θ, we can picture a right triangle, as shown in Fig. 1b, with a hypotenuse that runs between two ridges and along the direction of movement between the ridges (λ_2). We can then use geometry to find λ_2, which is the new effective spacing, as a function of the original spacing λ_1 and the angle between λ_1 and λ_2, which yields

$$\lambda_2 = \lambda_1/cos(\theta). \quad (2)$$

B. Using Effective Spacing to Estimate Slip Speed

Given the orientation in the form of the angle θ, as seen in Fig. 1b, and the center frequency of the fingerprint effect passband f_c, we can calculate the slip speed v of a surface

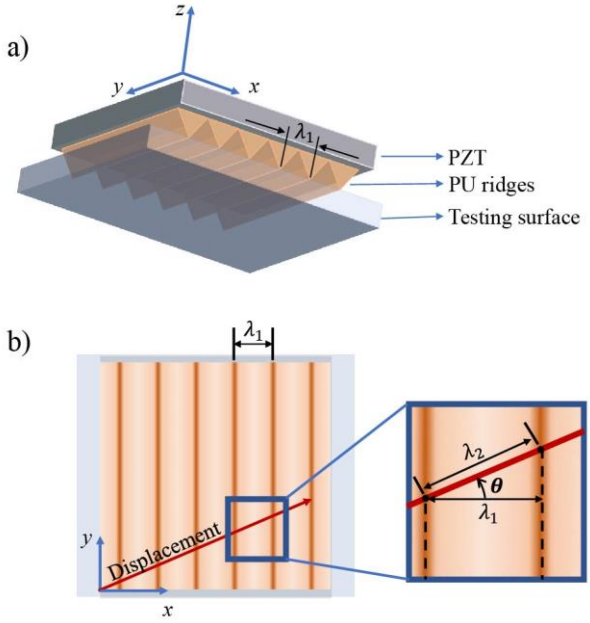

Fig. 1. Diagrams showing a) the cross section and spacing of fingerprint-like ridges on this paper's bioinspired sensor and b)) top view depiction of the fingerprint-like ridges in contact with the testing surface, darker lines representing contact. Ridge spacing changes when the direction of movement is changed by an angle θ.

across evenly spaced, parallel ridges by first using the effective spacing λ_2 in place of λ in eq. (1) to find

$$f_c = v/\lambda_2 = vcos(\theta)/\lambda_1 . \quad (3)$$

Then we can then use eq. (3) and rearrange terms to find

$$v = f_c\lambda_1/cos(\theta), \quad (4)$$

for $0° \leq \theta \leq 90°$. This can be extended to all angles θ by taking the absolute value of the cosine function, which gives

$$v = f_c\lambda_1/|cos(\theta)|. \quad (5)$$

We can also rearrange eq. (4) to find θ, which gives

$$\theta = cos^{-1}(f_c\lambda_1/v) \quad (6)$$

III. Materials and Methods

A. Sensor Fabrication

To test the dependence of the fingerprint effect on the orientation of fingerprint-like structures with respect to the direction of slip, a sensor was fabricated by layering microstructures with a thin backing on top of a soft, curved polymer surface, which was, in turn, on a lead zirconate titanate (PSI – 5H4E, Piezo.com), otherwise known as PZT, transducer. The sensor had straight, parallel ridges with a triangular cross section, a height of 200 µm, and a center-to-center spacing of 400 µm.

The sensor's transducer was prepared by first etching a 14 mm x 14 mm recessed square using a laser engraver (Laser Mini 30 W, Epilog), 100 µm deep, into an 18 mm x 18 mm x 1.6 mm piece of acrylic, creating a seat for the PZT. Another, 4 mm x 4 mm square was cut out of the corner of the acrylic seat, leaving space to solder a wire to the back electrode of the PZT. Then, a 14 mm x 14 mm x 270 µm square piece of PZT with nickel electrodes, was glued into the acrylic seat using superglue (Loctite 404). Wires were then soldered to both sides of the PZT square and the open back portion of the PZT was reinforced with superglue (Loctite 404). After that, a silicone rubber (Mold Max 30, Smooth On) mold was used to place a 1 mm thick layer of polyurethane (M-3115, BJB Enterprises) on the PZT transducer. This layer acted both as a soft backing and a way to cover the wire soldered to the top of the PZT.

As can be seen in Fig. 2, the straight, parallel ridges were fabricated using a silicone rubber (Mold Max 30, Smooth On) mold made from a positive machined from acrylic. Polyurethane (TC – 9445, BJB Enterprises) was then poured into the mold and an acrylic plug was used to ensure a backing that is approximately 200 µm thick. After the polyurethane cured, the plug was removed from the mold, taking the ridges out with it, and the ridges were then separated from the plug. TC – 9445 does not adhere to acrylic, so the ridges were then pealed from the plug with relative ease.

The microstructures were placed face down, backing up, on a 12 mm thick, flat piece of silicone rubber (Mold Max 30, Smooth On). Then a few drops of the soft polyurethane (M-3115, BJB Enterprises) that was molded onto the transducer were placed on the microstructure backing. After that, the PZT transducer in the acrylic seat was placed, polyurethane down, on top of the drops of polymer. The

stack of silicone rubber, microstructures with backing, uncured polymer, and cured polyurethane on PZT in the acrylic seat, were then placed in a vertical vice and compressed. The sensor was then left for 24 hours the polyurethane to cure. This compression process causes the uncured polyurethane to take on a slight curvature because of the deformation profile of the soft silicone rubber surface under uniform compression, which is similar to the deformation profile of an elastic half-space under finite uniform pressure [11]. The resulting curve helps to ensure contact between consecutive microstructures and a surface, and helps alleviate alignment errors. The final fabricated sensor can be seen in Fig. 2b along with a magnified view of the ridges. Fig. 2c shows the ridge ends from a side view, demonstrating the triangular cross section.

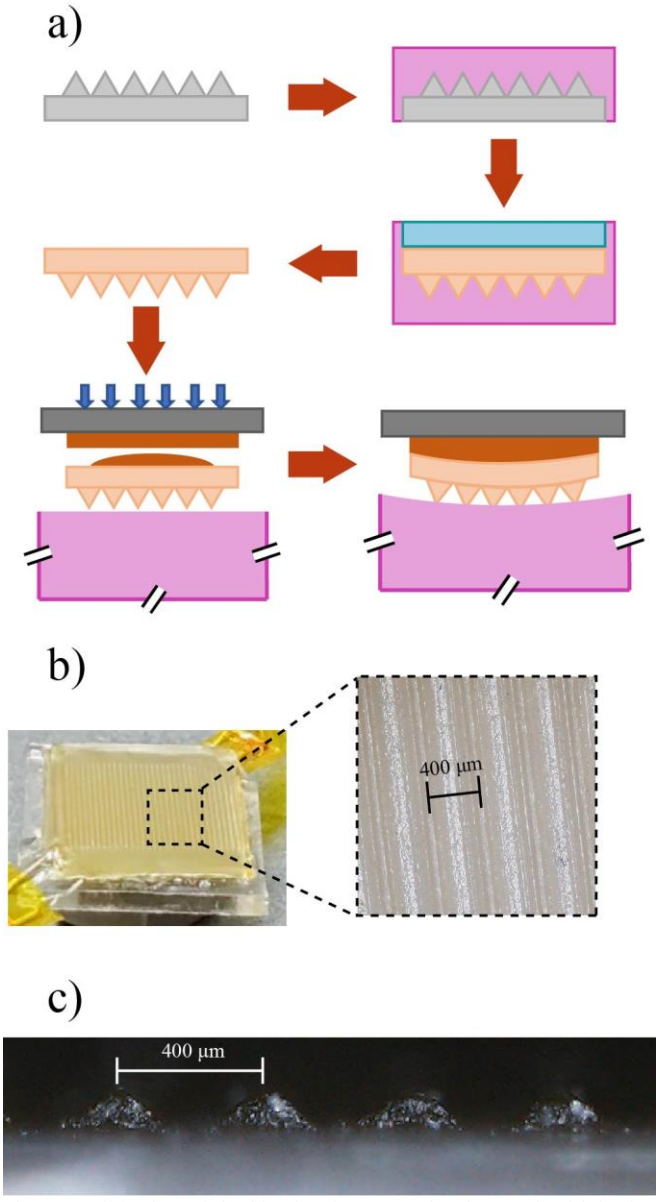

Fig. 2. Fabrication of the biomimetic sensor showing a) the fabrication process starting with micro-milling of the ridge structures from an acrylic plate, creating a silicone rubber mold, casting the silicone rubber mold with polyurethane, removing the polyurethane ridge structure from the mold, placing the ridges on a relatively large and soft silicone rubber surface, and applying liquid polyurethane at the back of the ridge structure and pressing the PZT to adhere it to the ridges. b) The fabricated sensor with a magnified view of the ridges. c) A magnified view of ridge ends showing the triangular cross section.

B. *Test Surface Fabrication*

The test surface was fabricated by imprinting polyurethane with a 120-grit sandpaper. Sandpaper was chosen because it meets standards defined for grain size distributions, which helps ensure a uniform distribution of surface feature sizes without a pattern. A coating of mold release agent (Ease Release 200, Mann Release Technologies) was applied to the sandpaper. Then, a layer of a relatively hard Shore D polyurethane (TC-9445, Hardness Shore D 45, BJB Enterprises) was poured onto a 3 in x 2 in x 1.2 mm glass slide. The abrasive side of the sandpaper was then pressed into the polyurethane layer. Another glass slide was placed on the sandpaper to ensure an even distribution of pressure. A 1 kg weight was placed on top of the second slide. The polyurethane was then allowed to cure for 24 hours. When the sandpaper was subsequently removed, its imprint remained in the polyurethane, creating a test surface comprised of a rough polyurethane surface on top of a glass slide. Note that since the polyurethane was cured on the glass slide, the two are bonded well enough to allow for testing without delamination.

C. *Test Setup*

The experimental setup used to test the fingerprint sensors can be seen in Fig. 3. To simplify the testing process, rather than moving sensors across a test surface, the test surface was moved across the sensor. This was accomplished by mounting the test surface on a motorized stage (X-LHM100A-E03, Zaber Technologies), while the sensor was mounted on a custom stage/load cell assembly. The motorized stage was mounted on a rotation stage (M-481-A High Performance Rotation Stage, Newport Corporation) through a custom 1 cm thick aluminum adapter. The rotation stage was mounted on a breadboard table (PG^{tm} Series Sealed Hole Breadboard, Newport Corporation). The

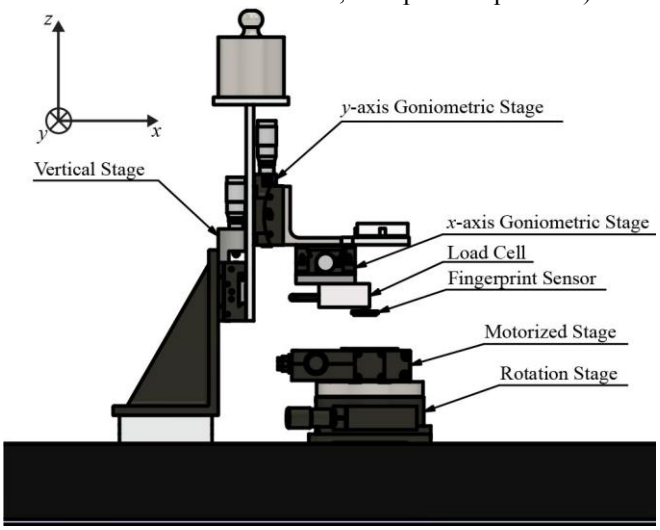

Fig. 3. Experimental test setup

base of the custom structure for mounting the sensor consisted of a right-angle aluminum bracket (360-90 angle bracket, Newport Corporation) mounted to the previously mentioned vibration table through a 0.75 in thick custom acrylic spacer. A linear stage (9065-Z vertical linear stage, Newport Corporation) was mounted vertically on the bracket. This stage was kept unlocked and its micrometer was moved out of contact with it, allowing free movement up and down. A goniometric stage (GON40-L goniometric stage, Newport Corporation) was mounted to the linear stage through a 5 mm thick acrylic interposer. This goniometric stage was oriented vertically such that it rotated around the *y*-axis (refer to Fig. 3 for the coordinate system). The acrylic interposer also had a platform for adding weight to the linear stage, which caused it to move down towards, and press against, the test surface. A custom machined right angle aluminum bracket was used to mount a horizontally oriented goniometric stage (GON40-U goniometric stage, Newport Corporation) to the vertically oriented goniometric stage. The horizontal goniometric stage was oriented such that it rotated around the *x*-axis. The goniometric stages were originally included in the test setup as a precaution to maximize contact between the sensor and the test surface in the event that the surface and the sensor are misaligned. However, this ultimately proved unnecessary. An acrylic platform with a small electronic breadboard was mounted to the back of the horizontally oriented goniometric stage. A 500 gram load cell (GSO-500, Transducer Techniques) was mounted through a 5 mm thick acrylic interposer to the horizontally oriented load cell. A 6-32 screw with a ball bearing glued to its head with superglue (Loctite 404) was screwed into the load cell stem threads. The sensor was glued to the ball bearing using superglue (Loctite 404).

The procedure for gluing the sensor to the ball bearing begins by applying a small droplet of glue to the ball bearing. The sensor is then placed on the test surface in the desired orientation. This creates a natural alignment between the sensor and the test surface. The vertical linear stage is then lowered until the droplet of glue meets the back of the sensor. The glue is then allowed to set. In this way, the sensor is held in alignment with the test surface.

The sensor output was read through a charge amplifier (Brüel and Kjær type 2634 charge amplifier) with a gain of 0.2 mV/pC, which was powered by a power supply (BK Precision 1672 triple output DC power supply). The charge amplifier's output was read by an oscilloscope (Infinii Vision DSO-X 2014A, Agilent Technologies). The load cell output was read through a signal conditioner (TMO-2 load cell signal conditioner, Transducer Techniques) by the oscilloscope. The oscilloscope and motorized stage were controlled by a custom LabVIEW (National Instruments) program.

D. Experiments

Two sets of experiments were run to verify the effect of fingerprint-like structure orientation on the fingerprint effect and slip speed estimation. First, we verified the effect of speed on the fingerprint effect. Given eq. (1), and previously verified by others [12][13], we expect the center frequency f_c of the fingerprint effect to increase with increasing slip speed. To verify this, the sensor was oriented such that the direction of the motion of the motorized stage was perpendicular to its ridges. Weight was added to the acrylic interposer until the load cell measured output was 3.0 V, which corresponds to 150 g and which, in turn, corresponds to a compressive force measurement of 1.5 N. Since the vertical stage was left unlocked and out of contact with its micrometer, the compressive force stayed relatively constant during tests, despite large scale changes in the thickness of the test surface. While maintaining a constant pressure is not a necessary condition of the fingerprint effect, it can affect the magnitude of the vibrations elicited [14]. The motorized stage was then moved forward and backward and the resulting output of the sensor's PZT transducer was recorded on the oscilloscope through the charge amplifier. As such, all results are reported in Volts. This test was performed for 15 mm/s over a distance of 20 mm, 20 mm/s over a distance of 20 mm, and 25 mm/s over a distance of 25 mm.

The second experiment was intended to demonstrate the relationship between orientation and the fingerprint effect. It consisted of rotating the motorized stage, and thus the test surface, by 15º increments between 0º and 90º. The speed of the stage was kept at 25 mm/s over a distance of 25 mm and the initial compressive force measured by the load cell was 1.5 N for all the tests in this experiment.

Performing the FFT over such a large time interval helps to create a situation where the maximum magnitude is not necessarily at the center of the visible pass band. However, rather than attempt to identify a passband and denote its center frequency at f_c, we have instead elected to assign the maximum value in the passband of the fingerprint effect to f_c. We chose this approach both because it makes it easy to create an algorithm to identify f_c for the purpose of speed estimation and because experiments analyzed using this approach matched results previously reported by other researchers.

All results recorded in the experiments were analyzed using MATLAB. This includes a 6^{th} order high-pass Butterworth filter with a cutoff frequency of 15 Hz that was applied to each dataset. This filter was applied to the data because the magnitude of low frequency vibrations elicited by the movement of the sensor across a surface, specifically frequencies around and below 15 Hz, is often greater than the magnitude of vibrations caused by the fingerprint effect. While these vibrations are not necessarily noise, they are not related to the fingerprint effect, so we have chosen to filter them out.

IV. Results and Discussion

A. Speed Tests

Results from the speed tests can be seen in Fig. 4. Both time and frequency domain results are shown. Results are all from the same direction of movement (backward in a forward and backward set of movements). It has been

demonstrated that frictional forces acting on a human fingerprint in contact with a surface are dependent on direction [15]. This tends to result in more stick-slip and other disruptive behaviors in one direction (forward or backward) and better sliding in the other. While results for the speed tests were good for both directions, the selected direction were higher in magnitude. The results for a slip speed of 15 mm/s can be seen in Fig. 4a and Fig. 4d respectively. Fig. 4a shows the time domain results over the time of slip. Fig. 4d shows a fast Fourier transform (FFT) of the results in Fig. 4a. Fig. 4d, shows a peak at 37.5 Hz and several harmonics. Fig. 4b and Fig. 4e show, respectively, the time and frequency domain results for a slip speed of 20 mm/s. Fig. 4b shows the time domain results over the time of slip. Fig. 4e shows an FFT of the results in Fig. 4b. Fig. 4e shows a peak at 50.0 Hz along with several harmonics. Fig. 4c and Fig. 4f show, respectively, the time and frequency domain results for a slip speed of 25 mm/s. Fig. 4c shows the time domain results over the time of slip. Fig. 4f shows an FFT of the results in Fig. 4c. Fig. 4f shows a peak at 66.0 Hz plus several harmonics.

These tests verified the results of other researchers [12][13]. Using eq. (1) we can calculate the expected center frequency f_c of the fingerprint effect filter for each speed. For 15 mm/s we expect an f_c of 37.5 Hz, for 20 mm/s we expect an f_c of 50 Hz, and for 25 mm/s we expect f_c to be 62.5 Hz. Fig. shows peaks at 37.5 Hz, 50.0 Hz, and 66.0 Hz for 15 mm/s, 20 mm/s, and 25 mm/s respectively. The data for each speed also show a number of additional peaks that are harmonics of these fundamental frequencies. Spatial frequencies that are harmonics of the fundamental ridge frequency are also amplified by the fingerprint effect.

While f_c for 15 mm/s and 20 mm/s match the predicted value exactly, the f_c of 25 mm/s is higher than predicted by 3.5 Hz. Given how well established the fingerprint effect is, this deviation is almost certainly due to a mismatch between the speed or spacing used to calculate f_c and the actual values. The good match between predicted and actual f_c for the other two speeds, implies that the correct spacing value was used. Most likely, the ability of the stage to maintain a consistent and accurate speed is reduced at higher speeds. If we use eq. (4) with a θ value of 0º and a spacing λ_I of 400 µm to calculate a speed v that would correspond to an f_c of 66.0 Hz, we find that v is 26.4 mm/s, which is just under 6% greater than expected. Despite this discrepancy, 25 mm/s was the speed chosen for the orientation tests because, at all orientation tested, it produced values of f_c that were greater than the 15 Hz cutoff of the Butterworth filter applied to the data. Even without the filter, it is not possible to identify the fingerprint effect in the low frequency vibrations suppress by the filter.

B. Orientation Tests

Frequency domain results from the orientation tests can be seen in Fig. 5 and Fig. 6. For these tests, the data is taken from the direction (forward or backward) that produced the best results at each rotation angle. The direction was backward for 0º, 30º, 45º, 60º, and 90º and forward for 15º and 75º. Fig. 5 shows results for the test at 0º rotation, which is a new test repeating the test seen in Fig. 4c and Fig.

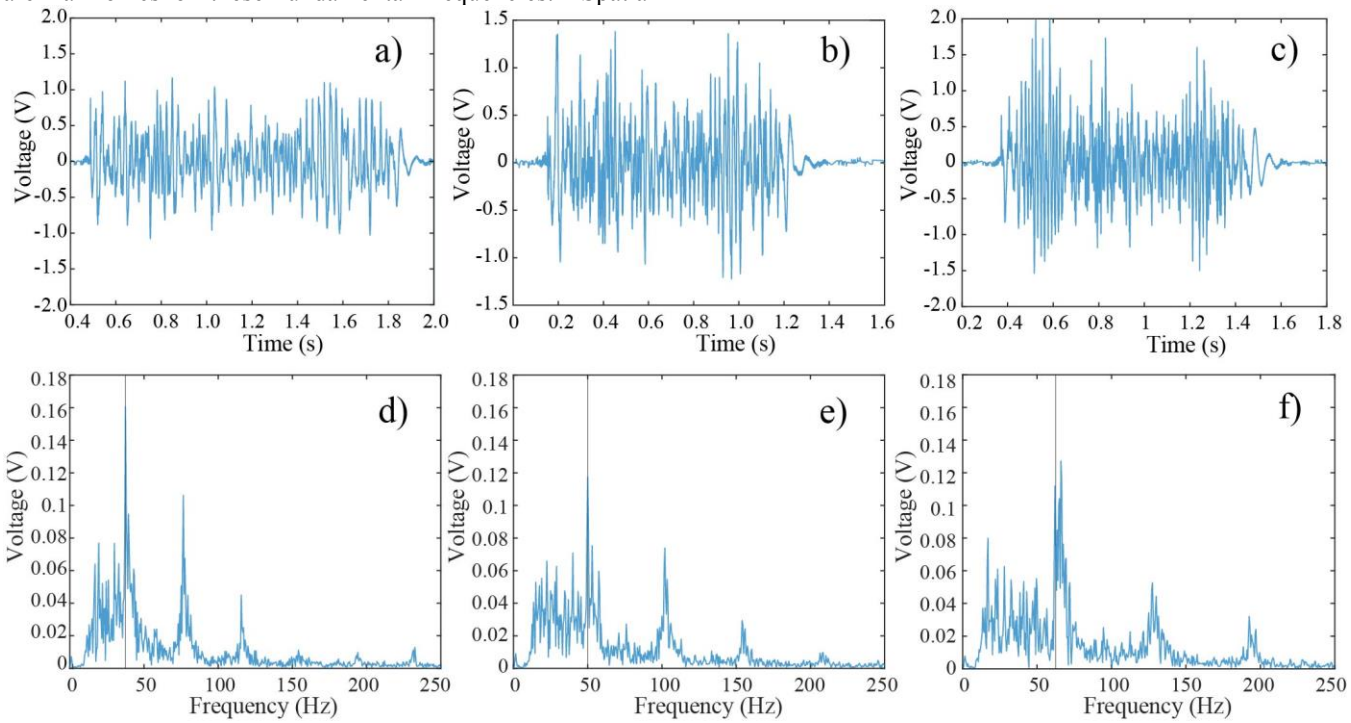

Fig. 4. Speed test results for a) 15 mm/s slip speed (time domain) b) 20 mm/s slip speed (time domain) c) 25 mm/s slip speed (time domain) d) 15 mm/s slip speed (frequency domain) e) 20 mm/s slip speed (frequency domain) and f) 25 mm/s slip speed (frequency domain).

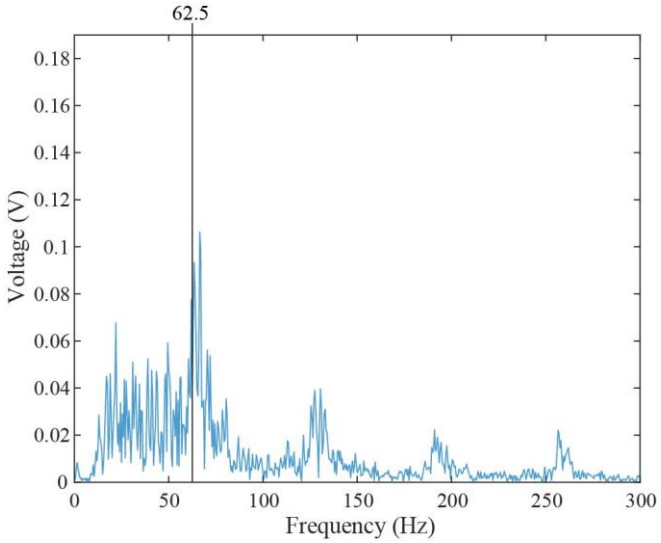

Fig. 5. Orientation test results (frequency domain) for 25 mm/s slip speed with a 0º rotation angle.

4f. There is a peak at 66.5 and several harmonics. Fig. 6 shows frequency domain results for tests from 15º to 90º. Fig. 6a shows the results for the test at 15º rotation. There is a peak at 61.0 Hz as well as harmonics. Fig. 6b shows the results for the test at 30º rotation. There is a peak at 58.0 Hz and harmonics. Fig. 6c shows the results for the test at 45º rotation. There is a peak at 48.5 Hz that is followed, again, by harmonics. Fig. 6d shows the results for the test at 60º rotation. There is a peak at 32.0 Hz. Fig. 6e shows the results for the test at 75º rotation. There is a peak at 19.0 Hz as well as what appears to be a single harmonic. Finally, Fig. 6f shows the results for the test at 90º rotation. There appears to be a prominent peak visible at 17.5 Hz. It is, however, worth noting that the magnitude of this peak is only 0.028 V, which is much smaller than the tallest peaks in any of the other tests. The appearance of a peak at 17.5 Hz is the result of the 15 Hz high pass Butterworth filter run on the data. Without the filter, the amplitude would be in constant decline starting at 0 Hz. It seems, therefore, safe to say that this is not caused by a fingerprint effect associated with the ridges of the sensor.

These tests show a good match between measured center frequencies f_c and those predicted by eq. (3) given the rotation angles involved. The calculated values of f_c are marked by a black line on each graph. The value of f_c, 66.5 Hz, from the first test, where θ is 0º, establishes a baseline speed v of 26.6 mm/s. Using this speed with eq. (3) and a spacing λ_1 of 400 µm, we can calculate center frequencies f_c for θ values of 15º, 30º, 45º, 60º, 75º, and 90º to be 64.2 Hz, 57.6 Hz, 47.0 Hz, 33.3 Hz, 17.2 Hz, and undetermined but approaching 0 Hz, respectively. These are all quite close to the largest peaks seen in Fig. 7, which are 61.0 Hz, 58.0 Hz, 48.5 Hz, 32.0 Hz, and 19.0 Hz for 15º, 30º, 45º, 60º, and 75º respectively. The calculated values vary from the measured values by 6.4%, 5.2%, 0.6%, 3.1%, 4.1%, and 8.6% for 0º, 15º, 30º, 45º, 60º, and 75º respectively. At 90º, f_c should be indistinguishable from 0 Hz and, as was previously mentioned, there does not appear to be any fingerprint effect present in Fig. 7f.

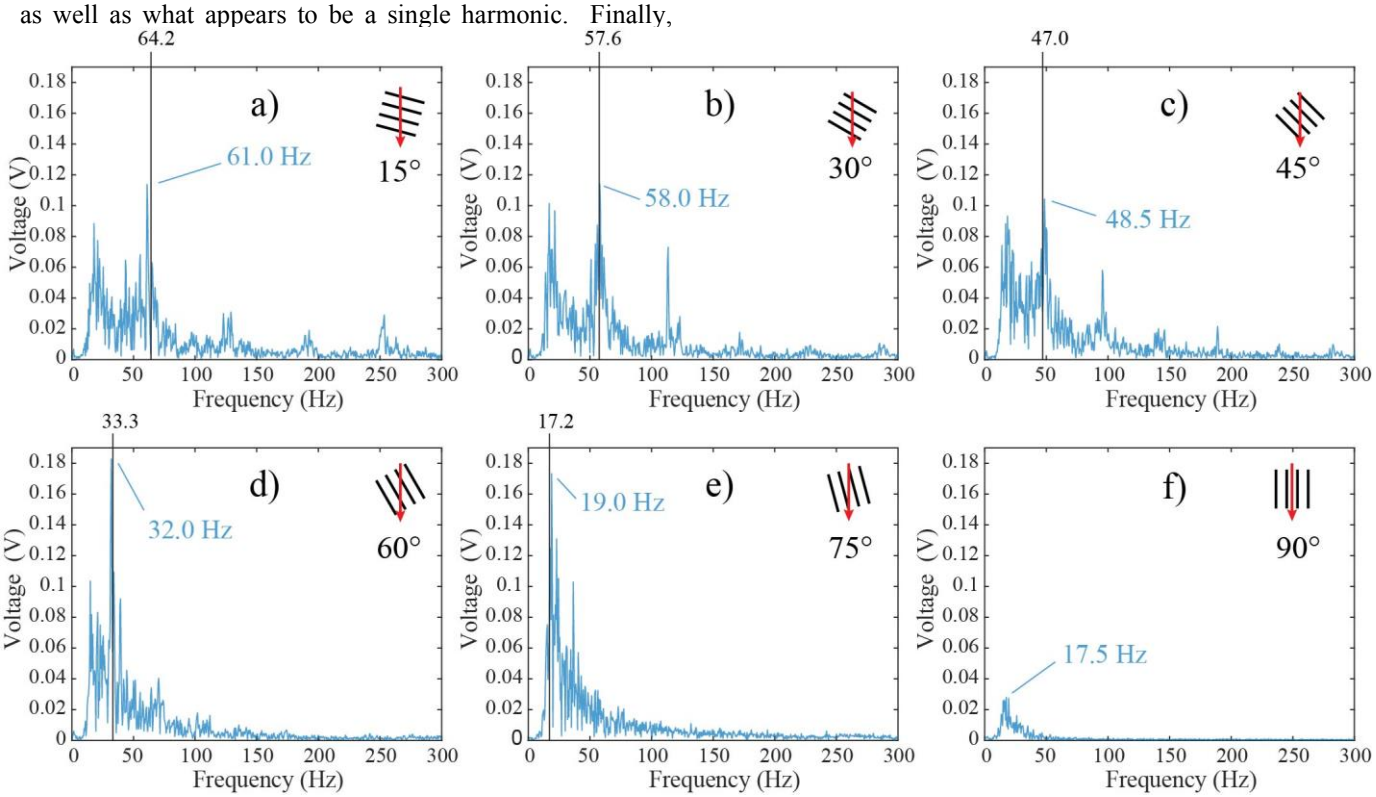

Fig. 6. Orientation test results (frequency domain) for 25 mm/s slip speed with rotation angles of a) 15º b) 30º c) 45º d) 60º e) 75º and f) 90º.

C. Simulation of Real-Time Slip Speed Estimation

If the peak in the frequency spectrum corresponding to the fingerprint effect can be identified, finding slip speed is as simple as applying eq. (5). While guaranteeing the robustness of an algorithm for identifying f_c would likely require a more advanced method, we will briefly discuss a simple algorithm that demonstrates a basic ability to estimate slip speed.

Since active touch involves some preexisting understanding of sensor velocity, a robot already has preconceived values for direction (i.e. θ) and speed v. To use the frequency response of the sensor to calculate v, a high-pass filter and maximum magnitude approach can be used. While, due to the high pass Butterworth filter, it is not visually obvious in our results, there is always a great deal of energy in the low frequency vibrations output by a sensor utilizing the fingerprint-effect. The best cutoff frequency for the high-pass filter is speed dependent, with higher frequencies required for higher speeds. For our example here, some trial and error showed that 25 Hz was a good choice for eliminating low frequencies that can have greater magnitude than f_c. It is important to note that according to eq. (6), at 25 mm/s, this filter will cut off f_c at rotation angles above 66.4º.

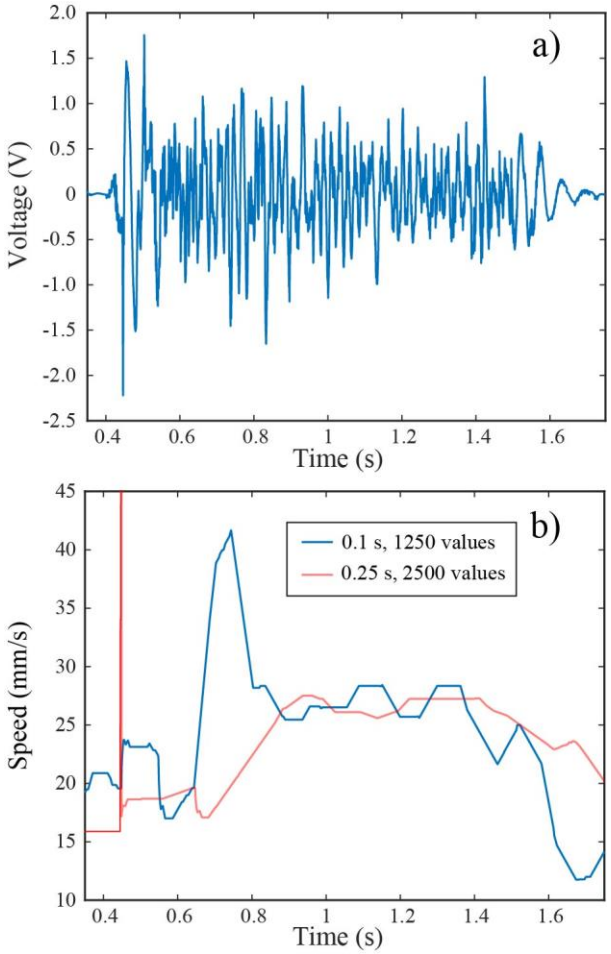

Fig. 7. Results of slip speed estimation for 45º rotation with speed set to 25 mm/s. Shown are a) original signal b) maximum magnitude algorithm results with 0.1 s window and 1250 maximums averaged per point (blue) and 0.25 s window and 2500 maximums averaged per point (red).

To model real-time speed estimates, a sliding window was applied to the time domain data. The window moved 8 x 10^{-5} s at a time, which is the sampling period, so each new window moves forward by one time sample. In real applications, a larger time step might be necessary to allow for all calculations. The data in the window was run through the high pass filter and then an FFT. The maximum magnitude value was then found, and its corresponding frequency was noted as f_c. This value was then averaged with previous f_c values and plotted against the highest time value of the window. The result of running this algorithm using the time data collected at 45º rotation for this paper can be seen in Fig. 7. Fig. 7a shows time domain data for comparison to the speed estimations. Fig. 7b shows speed estimation using a 0.1 s window and averaging the last 1250 values of f_c (blue) and using a 0.25 s window and averaging the last 2500 values of f_c (red).

In both simulations, the vibrations seem to be detected rapidly after they start around absolute time 0.4 s. However, it takes about 0.4 s from when vibrations start for the calculated speed to settle around 25 mm/s. We believe that the time delay between the beginning of vibrations and the accurate estimating of slip speed has three primary causes. First, before accurate estimations can occur, the time window must include enough vibrations for the frequency associated with the fingerprint effect to have the highest magnitude in the FFT. Second, averaging the speed estimates over time has a lowpass filter effect on the speed estimation data, which means that the speed estimated by the algorithm is limited in how fast it can change. Rise time between first detection of vibration and accurate estimation of slip speed is, therefore, dependent on the number of values being averaged. Finally, visual inspection of the voltage output of the sensor shows that the vibrations seem to start with a jolt when the surface begins to slide, followed by some high frequency vibrations before settling into vibrations that seem to have a more consistent frequency. This implies that there are either transient vibrations created by the initialization of slip which mislead the speed estimation algorithm, or that the speed itself is varying and then settling into the desired speed of 25 mm/s and the algorithm, particularly when using a 0.1 s window and averaging 1250 samples, is accurately estimating the speed with delay caused only by the first two sources listed.

These results show that there are tradeoffs associated with the size of the window and the number of f_c values being averaged. In both cases, larger numbers smooth out the speed results, but the estimation will lag farther behind the leading edge of the window. The smoothing is the result of bigger windows having smaller frequency increments and averaging more values of f_c, which compensates for deviations of short duration. Fig. 7 shows some clear variation in frequency over time, particularly early on. This variation is better reflected in 0.1 s window results than the 0.25 s window results. Thus, the optimal choices of window size and number of values of f_c to average are application dependent. While methods for determining ideal parameters

for different applications should be developed, they are beyond the scope of this work.

V. Conclusion

This paper has demonstrated both theoretically and experimentally that the fingerprint effect is orientation dependent and that, if the orientation is known, it can be used to estimate slip speed. This has implications for slip dependent robotics applications such as texture sensing and controlled slip. It shows the importance of both controlling slip direction, with respect to fingerprint-like structures, when possible, and knowing that direction when control isn't possible. Also, for applications where knowledge of slip speed is desired, it is possible to use the fingerprint effect and a simple algorithm to estimate slip speed. While such simple algorithms can fall victim to numerous sources of error, they can still provide vital support when slip speed is estimated using a synthesis of data from multiple sensor types. Also, more complex algorithms or machine learning might prove more robust.

Also of note, eq. (3) makes it apparent that, if both speed and orientation are unknown, it is impossible to know which of the two has caused a given change in the center frequency f_c of the fingerprint effect. This suggests that any algorithm that relies on the fingerprint effect alone for speed estimation should incorporate orientation to minimize error.

The work in this paper also suggests that it is important to evaluate the effect of orientation on slip sensors using other fingerprint-like structures. We have discussed how straight, evenly spaced, parallel ridges behave similarly to evenly spaced, curved ridges with a sufficiently large radius of curvature. However, multiple other fingerprint-like structures, such as pillars, bumps, and curved ridges with small radii of curvature have been used in tactile sensors. These structures could all benefit from a similar analysis in future work.

References

[1] J. Scheibert, S. Leurent, A. Prevost, and G. Debrégeas, "The Role of Fingerprints in the Coding of Tactile Information Probed with a Biomimetic Sensor," *Science,* vol. 323, no. 5920, pp. 1503-1506, 2009 2009, doi: 10.1126/science.1166467.

[2] Y. Jiang, Z. Ma, B. Cao, L. Gong, L. Feng, and D. Zhang, "Development of a tactile and slip sensor with a biomimetic structure-enhanced sensing mechanism," *Journal of Bionic Engineering,* vol. 16, no. 1, pp. 47-55, 2019.

[3] L. R. Manfredi *et al.*, "Natural scenes in tactile texture," *Journal of neurophysiology,* vol. 111, no. 9, pp. 1792-1802, 2014.

[4] Y. Cao, T. Li, Y. Gu, H. Luo, S. Wang, and T. Zhang, "Fingerprint-inspired flexible tactile sensor for accurately discerning surface texture," *Small,* vol. 14, no. 16, p. 1703902, 2018.

[5] W. Navaraj and R. Dahiya, "Fingerprint-enhanced capacitive-piezoelectric flexible sensing skin to discriminate static and dynamic tactile stimuli," *Advanced Intelligent Systems,* vol. 1, no. 7, p. 1900051, 2019.

[6] Y. Massalim, Z. Kappassov, and H. A. Varol, "Deep Vibro-Tactile Perception for Simultaneous Texture Identification, Slip Detection, and Speed Estimation," *Sensors,* vol. 20, no. 15, p. 4121, 2020.

[7] A. Prevost, J. Scheibert, and G. Debrégeas, "Effect of fingerprints orientation on skin vibrations during tactile exploration of textured surfaces," *Communicative & integrative biology,* vol. 2, no. 5, pp. 422-424, 2009.

[8] G. Chimata and C. J. Schwartz, "Investigation of friction mechanisms in finger pad sliding against surfaces of varying roughness," *Biotribology,* vol. 3, pp. 11-19, 2015.

[9] C. M. Oddo, L. Beccai, J. Wessberg, H. B. Wasling, F. Mattioli, and M. C. Carrozza, "Roughness Encoding in Human and Biomimetic Artificial Touch: Spatiotemporal Frequency Modulation and Structural Anisotropy of Fingerprints," *Sensors,* vol. 11, p. 20, 2011, doi: 10.3390/s110605596.

[10] E. Wandersman, R. Candelier, G. Debrégeas, and A. Prevost, "Texture-induced modulations of friction force: the fingerprint effect," *Physical review letters,* vol. 107, no. 16, p. 164301, 2011.

[11] S. P. Timoshenko and J. N. Goodier, "Theory of elasticity," 1951.

[12] C. M. Greenspon, K. R. McLellan, J. D. Lieber, and S. J. Bensmaia, "Effect of scanning speed on texture-elicited vibrations," *Journal of The Royal Society Interface,* vol. 17, no. 167, p. 20190892, 2020.

[13] R. Fagiani, F. Massi, E. Chatelet, Y. Berthier, and A. Akay, "Tactile perception by friction induced vibrations," *Tribology International,* vol. 44, no. 10, pp. 1100-1110, 2011.

[14] R. Fagiani, F. Massi, E. Chatelet, J. P. Costes, and Y. Berthier, "Contact of a finger on rigid surfaces and textiles: Friction coefficient and induced vibrations," *Tribology Letters,* vol. 48, no. 2, pp. 145-158, 2012.

[15] X. Zhou, J. L. Mo, Y. Y. Li, Z. Y. Xiang, D. Yang, M. A. Masen, and Z. M. Jin, "Effect of Finger Sliding Direction on Tactile Perception, Friction and Dynamics," *Tribology Letters,* vol. 68, no. 3, pp. 1-13, 2020.